THE JOURNAL OF BIOLOGICAL CHEMISTRY VOL. 282, NO. 1, pp. 691–699, January 5, 2007
Printed in the U.S.A.

Structural Basis for p53 Binding-induced DNA Bending*[S]

Received for publication, June 20, 2006, and in revised form, September 27, 2006 Published, JBC Papers in Press, November 3, 2006, DOI 10.1074/jbc.M605908200

Yongping Pan[‡] **and Ruth Nussinov**[‡§1]

From the [‡]*Center for Cancer Research Nanobiology Program, SAIC-Frederick, Inc., NCI-Frederick, National Institutes of Health, Frederick, Maryland 21702 and* [§]*Sackler Institute of Molecular Medicine, Department of Human Molecular Genetics and Biochemistry, Sackler School of Medicine, Tel Aviv University, Tel Aviv 69978 Israel*

Specific p53 binding-induced DNA bending has important biological implications such as transcription activation. However, the detailed structures of the bent DNA and the p53-DNA complex are still unavailable, hampering our understanding of the mechanism for p53-induced DNA bending and its consequent biological significance. To gain insight into the p53 binding-induced DNA bending, we performed molecular dynamics simulations on DNA segments with the consensus sequence for p53-specific binding, half site DNA-p53 complexes, and full site DNA-p53 complexes. We show that each DNA-bound p53 core domain caused a local DNA conformational change within the quarter site; upon the binding of the p53 dimer, there was an apparent DNA bending at the center of the half site; when bound with two p53 dimers, the full site DNAs with two different sequences bent 20 and 35°, respectively. These results are in agreement with experimental observations. Our simulations demonstrate that the two p53 dimers favored a staggered conformation in which they make favorable interactions at the interface. This dimer-dimer interface organization necessitated conformational changes in the DNA, leading to the bending at the center of the full site, which in turn is dependent on the DNA sequence. Overall, our results provide the detailed atomic model for the DNA-p53 tetramer complex and delineate the roles of DNA-p53, p53 dimer-dimer interactions, and DNA sequence in specific p53 binding-induced DNA conformational changes.

In response to cellular stress such as DNA damage, tumor suppressor p53 is activated and functions as a transactivator to regulate several genes, preventing the development of cancer (1–4). A critical biochemical event for the p53 transactivation activity is its sequence-specific binding to DNA (5). p53 binding sites are usually composed of two 10-base pair (bp) repeats 5′-PuPuPuC(A/T)(A/T)GPyPyPy-3′, where Pu and Py stand for purine and pyrimidine bases, respectively (6–8); the two repeats can be separated by as many as 13 base pairs (7, 9). More than 100 different specific p53 response elements in the human genome that satisfy the consensus have been characterized (7). The variance of the DNA sequence and the consequent difference in p53 binding affinity were suggested to be important in deciding which target gene to activate. The p53 protein is a tetramer of four homologous peptide chains, with each chain composed of several domains including the N-terminal domain that regulates the p53 transactivation activity (10), the specific DNA-binding core domain (11), the tetramerization domain (12) that allows the equilibration between the tetrameric and other conformational states, and the C-terminal domain. It was shown that during the specific p53-DNA binding process, p53 first binds to the DNA non-specifically and then diffuses along the linear DNA duplex until it reaches the target sequence where the p53 core domain interacts with the DNA specifically (13). As a result, DNA experiences conformational changes such as axial bending (14–16) and the p53 exposes its acetylation motifs (17). Such a specific binding process has been shown to be highly cooperative in that both the oligomerization of p53 and the presence of the full p53 binding site are required (18, 19). The binding of the half site only or of the altered full site is very weak and non-cooperative (18, 20).

The overall organization of the p53 tetramer-DNA complex has been proposed by several groups based on crystal structures and other biophysical and biochemical data (11, 20–23) in which each of the four p53 core domains binds to a DNA quarter site in the same manner, with each pair of the core domains associated with one another through salt bridges at the H1 helix region, resulting in a symmetric arrangement of the p53 core domains. These specific ways of association between p53 and DNA and between p53 monomers are supported by several experiments (24–27). Alternatively, p53 core domain dimerization interface in a crystal structure was also examined to explore their biological relevance (28). Overall, there are little experimental data with respect to the association between the p53 dimers. Model building by mapping the four p53 domains onto the straight DNA consensus sequence suggested that such a dimer arrangement would incur some steric conflict between the dimers (23). As a result, the DNA has to bend as much as 50° to avoid direct repulsion and to allow favorable interactions between the p53 dimers (23). Recently, a crystal structure of two p53 dimer half site DNA stacked side by side was solved (29), showing the staggered interface between the dimers of p53. However, because the oligonucleotides used in the experiment are not continuous, the dimer-dimer interface incurred in the corresponding complex does not warrant the same organization when a continuous full site DNA is applied.

* This work was supported in part by the Intramural Research Program of the NCI, National Institutes of Health Center for Cancer Research and by the NCI under contract NO1-CO-12400. The research of R. Nussinov in Israel has been supported in part by the Center of Excellence in Geometric Computing and its Applications funded by the Israel Science Foundation. The costs of publication of this article were defrayed in part by the payment of page charges. This article must therefore be hereby marked "*advertisement*" in accordance with 18 U.S.C. Section 1734 solely to indicate this fact.

[S] The on-line version of this article (available at http://www.jbc.org) contains supplemental Figs. S1 and S2.

[1] To whom correspondence should be addressed: Bldg. 469, Rm. 151, Frederick, MD 21702. Tel.: 301-846-5579; Fax: 301-846-5598; E-mail: ruthn@ncifcrf.gov.

To gain insight into the p53-DNA interactions and the consequent DNA conformational changes, we systematically studied the structural properties of DNA alone, DNA-p53 monomer (DNA-p53m), DNA-p53 dimer (DNA-p53d), and DNA-p53 tetramer (DNA-p53t) complexes with molecular dynamics simulations based on the symmetric model. We show that the binding of the p53 monomer or dimer caused the DNA to bend at the center of the half sites. Upon the binding of dimer of dimers, the DNA bend 20 and 35° for two different DNA sequences, respectively, in qualitative agreement with the bending extent observed experimentally and consistent with other modeling results (30). The simulations results reveal that the two p53 dimers in the DNA-bound state adopted a slightly shifted conformation that allows the favorable interactions and packing at the p53 dimer-dimer interface and results in the bending of DNA.

MATERIALS AND METHODS

Model Construction—DNA alone and DNA-p53 complexes with one, two, and four copies of the p53 core domain were investigated in this study. All molecular models were derived from the crystal structure (Protein Data Bank code 1TSR) (11). The DNA segment and the B chain of p53 in the crystal structure that was bound to DNA specifically were directly extracted from the Protein Data Bank file as the DNA-p53 monomer model (DNA-p53m; Fig. 1*A*); the DNA-p53 dimer complex (DNA-p53d) was constructed by superimposing the base pairs from two copies of the DNA-p53m complex in reverse order and in a way that the superposition resulted in a DNA double helix with the two copies of p53 bound to two consecutive quarter sites of the DNA (Fig. 1*B*). The resulting DNA-p53 dimer complex (DNA-p53d) structure ensures the specific DNA-p53 binding and that the two copies of p53 have a C2 symmetry, with formation of the salt bridges between the H1 helices. The DNA-p53 tetramer (DNA-p53t) model was constructed by merging two copies of DNA-p53d such that the resulting DNA segment has a continuous p53 binding full site with no base pair insertions and the two dimers of p53 are side by side (Fig. 1*C*). Although other ways of p53 tetramer-DNA complex organizations are possible, the model used here focused only on the type of organization where the dimers are symmetrically positioned on the DNA with respect to each other, with each monomer bound to the DNA specifically, as observed in the crystal structure (11). The DNA sequence for the DNA-p53m and DNA-p53d complex simulation is 5′-ATT**GGGCA AGTCT**AGG-3′, extracted from the crystal structure. For the DNA-p53t complex simulations two DNA sequences were used, 5′-ATAATT**GGGCA AGTCT**‖**GGGCA AGTCT**AGGAA-3′, or the Cho sequence (11), and 5′-ATAATT**GAGCA TGCTC**‖**GAGCA TGCTC**AGGAA-3′, or the Ho sequence (31) with the base pairs for p53 binding site in bold. The second DNA-p53t model was obtained by mutating the base pairs in the first DNA-p53t model into the sequence used in previous experimental work (31).

MD Simulation Protocol—Each system was first solvated with a TIP3P water box (32) with a margin at least 10 Å from any edge of the water box to any protein or DNA atom. Solvent molecules within 1.6 Å of DNA or 2.5 Å of protein were removed. The systems were then neutralized by adding either sodium or chloride ions. The resulting systems were then subjected to a series of minimizations and equilibrations before the production of MD[2] simulations with the CHARMM program (33) and the CHARMM 22 force field (34). Minimizations were first performed for 500 steps with the steepest decent algorithm with the backbone of the core domain constrained and an additional 500 steps for the whole system to reduce the unfavorable interactions. The systems were further pre-equilibrated for 20 ps with the NVT ensemble before the production simulations, which lasted for 10 ns with the NPT ensemble at temperatures of 300 K. Periodic boundary conditions were applied, and the non-bonded lists were updated every 20 steps. A time step of 2 fs and a nonbonded cutoff of 12 Å were used in the trajectory production. Electrostatic energies were calculated with the PME algorithm implemented in Charmm, and the order of 6 was specified for B-spline interpolation. Structures were saved every 2 ps for analysis.

RESULTS

Half Site DNA and Complex Simulations

DNA Intrinsic Properties and Conformational Changes upon p53 Binding—The 15-base pair DNA containing the consensus sequence (half site) was subjected to MD simulations by itself, in complex with one p53 core domain (DNA-p53m; Fig. 1*A*), and in complex with two p53 core domains (DNA-p53d; Fig. 1*B*). These simulations were designed to investigate the intrinsic DNA conformational preferences and the conformational changes upon p53 binding in the context of the half p53 binding site. Fig. 2 shows the DNA conformations for the three cases. The DNA apparently preferred a double helical conformation with a straight axis when it was not in complex with p53 (Fig. 2*A*). When DNA was in complex with either one or two p53 core domains, the axis of the DNA became slightly yet noticeably bent (Fig. 2, *B* and *C*). Only the quarter site that was bound with p53 in the DNA-p53m complex was bent, and both quarter sites were bent in the DNA-p53d complex. More specifically, the bending was located at the base pair that was absolutely conserved in the consensus sequence, corresponding to the 4th and 7th positions of the half site (indicated by *small arrows* in Fig. 2). The DNA bending caused by the binding of two p53 core domains was consistent with the experimental findings (31). A view through the DNA axis further reveals the deformation of the DNA. In free DNA, the double helix adopted a regular round shape, as expected. However, the double helical DNA took an oval-like shape when in complex with two p53 core domains (Fig. 2). This is reminiscent of the clamp-like action by the p53 dimer proposed earlier with the salt bridges between the H1 helices as a hinge. These results suggest that the interactions between p53 and the conserved G base at the 4th (upper chain G base) and 7th (lower chain G base) positions within the consensus sequence played a major role in triggering the DNA conformational changes. However, it should be noted that the extent of DNA bending was quite limited.

Analysis of the DNA helical parameters further revealed the details of the DNA conformational changes upon p53 binding.

[2] The abbreviation used is: MD, molecular dynamics.

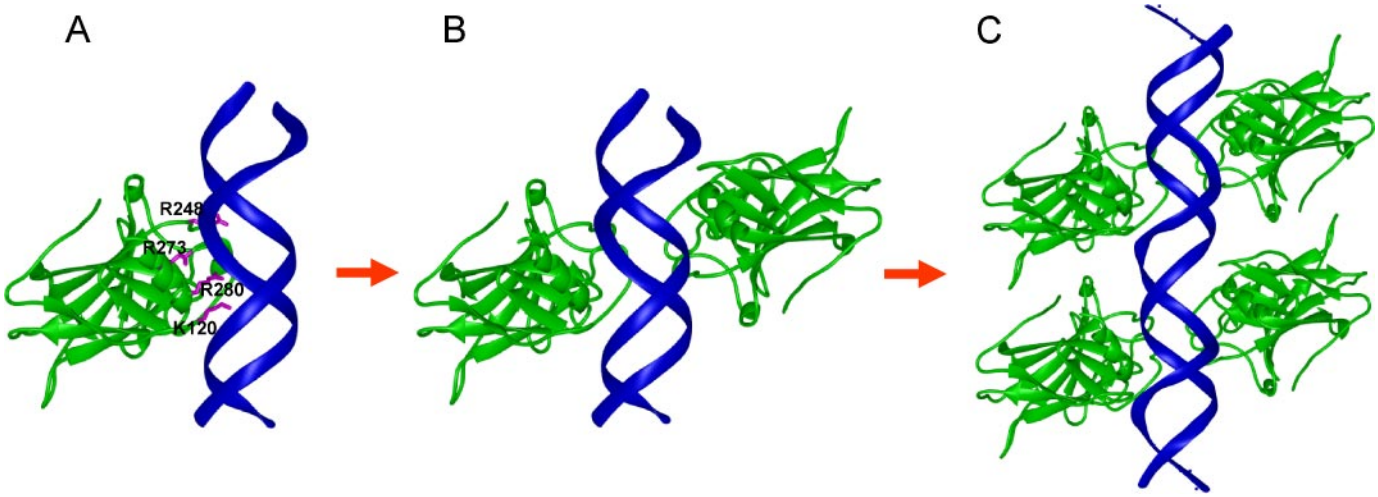

FIGURE 1. **DNA-p53 model complexes used in this study.** *A*, DNA-p53 monomer complex (DNA-p53m) derived from the crystal structure 1tsr. The B chain of the p53 that bound to DNA specifically was used, and the DNA segment was composed of bases 5–19 from the E chain and 4–18 from the F chain. Key residues involved in the specific DNA-p53 interactions are shown with Lys-120 (*K120*) and Arg-280 (*R289*) bound at the major groove forming hydrogen bonds and Arg-273 (*R273*) and Arg-248 (*R248*) to the minor groove backbone. *B*, DNA-p53 dimer complex (DNA-p53d), constructed by matching the DNA heavy atoms for the two copies of DNA-p53m so that the second p53 bound to DNA in the same manner as the first p53 and bears the D2 symmetry for the p53 dimer. *C*, DNA-p53 tetramer complex (DNA-p53t), built by connecting two copies of DNA-p53d so that the two DNA consensus half sites are next to each other without any base pair insertions. The DNA sequences used in these complexes were given under "Materials and Methods."

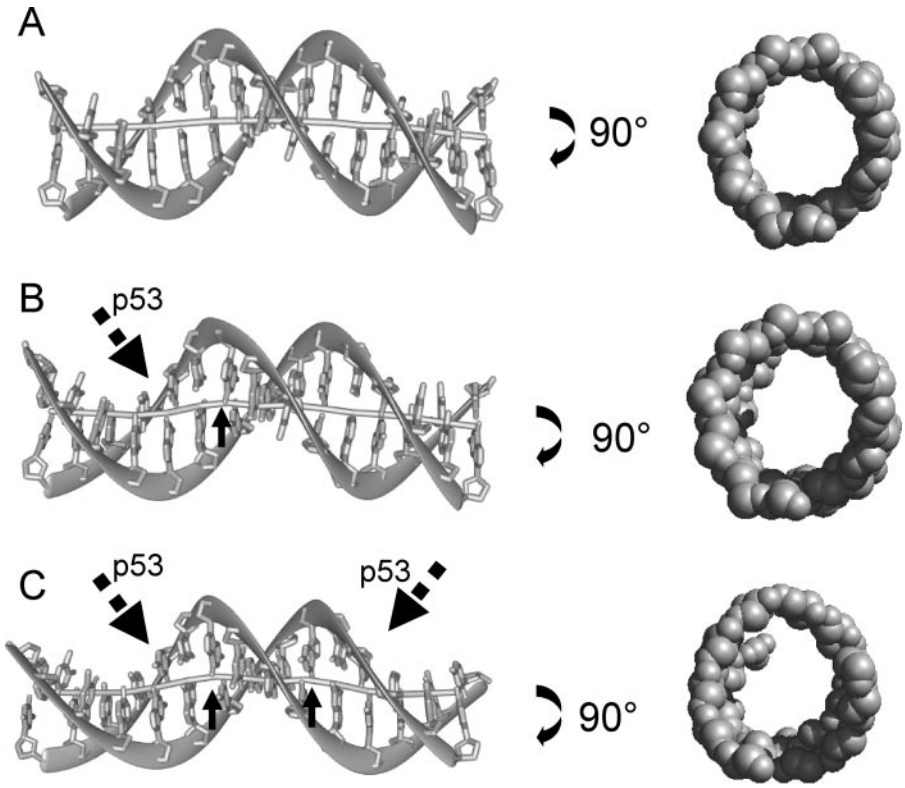

FIGURE 2. **Conformational changes of the 15-bp DNA segment upon p53 binding.** *A*, free DNA conformation. *B*, DNA conformation bound with one p53 core domain. *C*, DNA conformation bound with two p53 core domains. The conformations were averaged over the last 5 ns from the 10-ns MD trajectories. The DNA axes are shown for each conformation. P53 binding sites for DNA-p53m and DNA-p53d complexes and the DNA bending locations are indicated with *large* and *small arrows*, respectively. The *right panels* are the view through the DNA axis, and only the backbone of DNA is displayed to visualize the deformation.

Compared with the parameters of free DNA, it is noticeable that the major groove width became larger at the quarter site that was bound with p53, particularly at the 4th position (supplemental Fig. S1*A*, *red*) whereas the major groove depth became shallower at the 3rd and 4th positions in the first quarter site (supplemental Fig. S1*B*, *red*). The changes in the minor groove parameters showed opposite trends compared with those of the major groove. Note that the minor groove parameters for both quarter sites were affected by the binding of one p53 core domain. The effect on the second quarter site was likely caused by the interactions of Arg-248 and other residues (Fig. 1*A*). Overall, the difference in the helical parameters between free DNA and p53-bound DNA was correlated with the specific interactions between the DNA and p53, particularly the p53 interactions of Arg-280 with the G base at the 4th and 7th positions. These specific interactions seemed to have resulted in the major groove narrowing near the center of the half site.

Key Interactions Responsible for the DNA Conformational Changes—To further characterize the important interactions between DNA and p53, the specific interactions between the DNA and p53 (B chain) in the crystal structure (11) were analyzed first. Next, each of the base pairs in the consensus sequence were substituted with the other three bases, one position at a time with the conformation of the DNA retained, and the interactions re-evaluated for the mutants. These data were then compared with the results from the MD simulations for the DNA-p53 complexes.

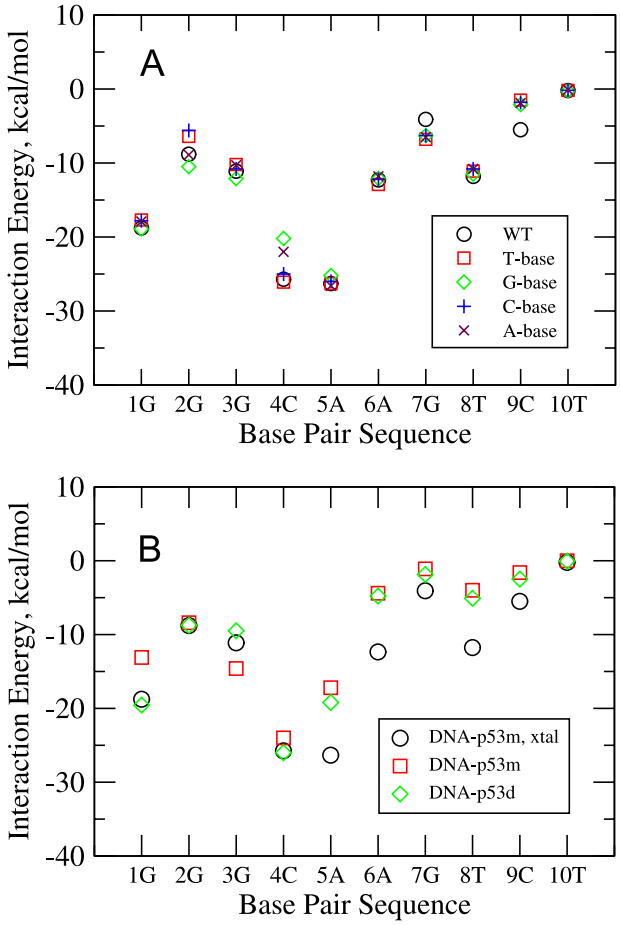

FIGURE 3. **The interaction energies between each base pair in the consensus sequence and p53 monomer in different conditions.** *A*, the interaction energies for the wild-type sequence in the crystal conformation and their changes upon base pair mutations. The conformation was taken directly from the crystal structure 1tsr for the wild type, and 1000 steps of energy minimizations with ABNR algorithm were performed for all the mutants to allow the DNA to accommodate the substituted base pair. *B*, the interaction energies for each base pair in the wild type averaged over the last 5 ns from the 10-ns MD trajectories for DNA-p53m (*red*) and DNA-p53d (*green*) complexes in comparison with the interaction energies from the crystal structure (*black*). In the DNA-p53d complex, only the interactions between DNA and one p53 core domain were calculated to facilitate the comparison. Nucleotide pairs, instead of base pairs, were used in the energy calculations.

The interaction energies for each base pair of the DNA consensus sequence with the p53 monomer in the crystal structure are shown in Fig. 3*A*. In this conformation, base pairs 1–5 and 6–10 were in contact with p53 through the major groove and minor groove, respectively. The interaction energies for the base pairs interacting through the major groove (bp 1–5) were in general more favorable than the corresponding energies for base pairs interacting through the minor groove (bp 6–10). Among the five base pairs of the first quarter site, the 2nd and 4th base pairs, which were second mostly and absolutely conserved, respectively (7), were sensitive to base pair replacement (Fig. 3*A*). When the pyrimidine base C at the 4th position was replaced with the other pyrimidine base T that is geometrically similar to C, the interaction energy was not or only slightly affected (Fig. 3*A*). However, when replaced with a purine base A or G, the interaction energy became much less favorable. The specific interaction of this bp with p53, which involves hydrogen bonding between the side chains of Arg-280 and the G base from the other DNA strand, was described in detail previously (11). Similarly, the interaction of the G base at the 2nd position, which made specific interactions with Lys-120, was only slightly affected when replaced with the other purine base, A, and became much less favorable when substituted with either a C or T. The other three positions (1st, 3rd, and 5th) were not sensitive to mutations, because only the backbones of these base pairs interacted with p53 and the conformation was essentially unaltered. Among the five base pairs of the second quarter site (bp 6–10), the most favorable interactions were between base pairs at the 6th and 8th positions and Arg-248 of p53 (11). The crystal structure shows that Arg-248 interacts with the phosphate backbones of these nucleotides. The side chain of Arg-248 was partially buried in the minor groove at the 8th position (Fig. 1*A*). Our results show that mutations at these two positions did not alter the interaction energy, consistent with the nonspecific backbone interactions. Interestingly, the interactions of base pairs at the 7th and 9th positions of the second quarter site deviated from the crystal structure, especially for the base pair at the 9th position. However, it did not make much difference whether the base pairs were replaced with a purine base or a pyrimidine base. Therefore, such a deviation of the interaction energy upon mutation may be related to conformational perturbation, not the direct disruption of specific interactions or the outcome of the mutations.

Next, the same interactions were analyzed from the molecular dynamics trajectories to compare their changes in the context of DNA-p53m and DNA-p53d complexes. Fig. 3*B* shows that only the interactions for base pairs at the 2nd, 3rd, and 4th positions essentially did not decrease. The strong interactions of the base pairs at the 2nd and 4th positions with p53 are supported by the high conservations and are consistent with the mutational results in Fig. 3*A*. These results demonstrate that the extensive interactions at the major groove, both specific interactions such as hydrogen bonding with the bases and nonspecific interactions with the backbones, helped maintain the strong interactions at the first quarter site; in contrast, because of the sparse contacts at the minor groove for the second site, these interactions were fragile and susceptible to changes in the environment. When DNA was bound to a p53 dimer, almost all the interactions became more favorable (Fig. 3*B*, *green*) relative to those for the DNA-p53m complex, suggesting that the dimerization, which was mediated by the salt bridge in the H1 helix motif, may have augmented the interactions between the DNA and each p53 monomer. The simulation results confirm that the interactions at the major groove were dominant and more stable than the interactions at the minor groove.

Full Site DNA and Complex Simulation

DNA Bending—As described under "Materials and Methods," the starting structure of the DNA in complex with four p53 core domains was almost linear (Fig. 4*A*). Each of the four copies of the p53 core domains binds specifically to a DNA quarter site of the 20-bp consensus sequence. For the complex with the Cho DNA sequence, after ~4.5 ns of production MD simulations, the DNA became bent with a bending angle of 20° (Fig. 4*B*). Further DNA bending was not observed in the simulation trajectory that was extended to 10 ns. In a parallel simu-

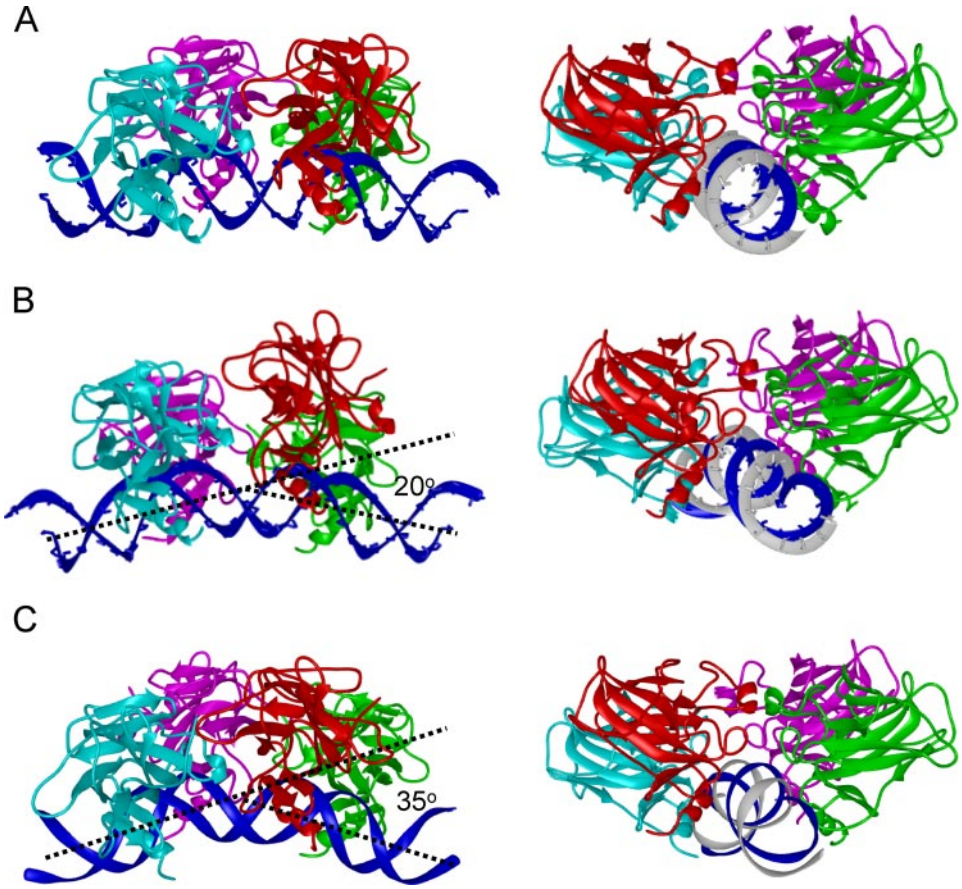

FIGURE 4. **DNA bending upon binding to p53 tetramer.** *A*, starting conformation for the MD simulation with two views perpendicular to each other. *B* and *C*, snapshots of the DNA-p53t complexes at 4.5 ns from the simulation involving the Cho DNA sequence and at 7.5 ns from the simulation involving the Ho DNA sequence, respectively. Two views perpendicular to each other are shown. The *left panels* show the DNA bending angle of 20 and 35° for the two DNA sequences, respectively, and the *right panels* present the p53 dimer shift with respect to each other.

lation with the Ho sequence of DNA, similar DNA conformational changes were observed (Fig. 4*C*). However, the DNA bending happened earlier with a much higher bending extent of 35° at 7.5 ns. This extent of DNA bending was maintained for the rest of the simulation trajectory. The magnitude of DNA bending observed here is in qualitative agreement with the experimental measurement for the p53 core domain-induced DNA bending, which could span a range from 20 to 45° under different conditions. In addition, the bending extents of the two DNAs also correlate with the different DNA flexibilities corresponding to the CAAG and CATG sequences at the middle of the half site.

To better characterize the DNA bending properties, the DNA helical parameters for the free DNA, constrained DNA, and the DNAs bound to the p53 tetramer were compared (supplemental Fig. S2). The 31-base pair-free DNA simulation (without constraint) yielded similar helical parameters across the 20-base pair consensus sequence (supplemental Fig. S2, *black*), which was typical for B-form DNA conformations. This result was expected but different from those of the shorter DNA simulations described earlier, indicating that the simulations can better reproduce the DNA conformational properties when a longer DNA segment is used. The helical parameters for the force-bent DNA show clear patterns of changes similar to the mathematical sine or cosine functions (supplemental Fig. S2, *green*). Interestingly, the peaks and the valleys for each of these parameters were one or two bases shifted from the centers of the half sites.

Comparison between those from the MD simulations of the DNA-p53t complex and those from the DNA that was bent by force showed a similar pattern for major groove parameters, particularly the major groove depth (supplemental Fig S2*B*). Because the parameters for the DNA bent by force were averaged over bending angles from 0 to 90° while the DNA bound with the p53 tetramer was only bent to a smaller extent, the differences in magnitude of the parameters were expected. However, the consistency in patterns between the major groove parameters for DNA bent by force and DNA bound with the p53 tetramer shows that the DNA preferred to bend at or near the centers of each half site for this particular binding site sequence (supplemental Fig. S2, *A* and *B*). For the minor groove, the pattern revealed in the force-bent DNA was not observed in the complex simulation, especially for the minor groove depth. In both simulation cases, the minor groove depth increased at the middle of the full site (supplemental Fig. S2*D*, *red* and *blue*). Given the short duration of the simulation and the weak interactions at the minor groove side, the discrepancy between the minor groove parameters was likely to be caused by the insufficient convergence.

To confirm that the DNA bending results from the forced bending and the DNA bending from the DNA-p53 complex simulations are reasonable, we compared them with data obtained for a representative DNA segment from a DNA loop crystal structure when bound with proteins (35). In this DNA segment the bending angle is ~60° (Fig. 5). The major groove parameters for this bent DNA were very similar to those of the DNA bent by force, not only in magnitude but also in patterns of changes, supporting the results obtained from the force-induced DNA bending. The crystal structure of the bent DNA clearly shows that the region bent the most corresponded to base pairs with the deepest major groove (Fig. 5). In the DNA-p53t complex model, this corresponds to positions near the center of the half sites, consistent with the notion that the A/T-rich regions have the tendency to bend. Thus, the observed DNA conformational change in our simulations was reasonable.

p53 Dimer-Dimer Interactions—The two dimers of p53 sat on the DNA side by side in the starting structure of the complex for the simulation (Fig. 4*A*). Because canonical B-form DNA

takes 10.5 base pairs to make a complete helical turn, two dimers bound to two consecutive 10-bp half sites will assume a slightly staggered conformation with the front dimer shifted to the right with respect to the second dimer (Fig. 4*A*, *right panel*).

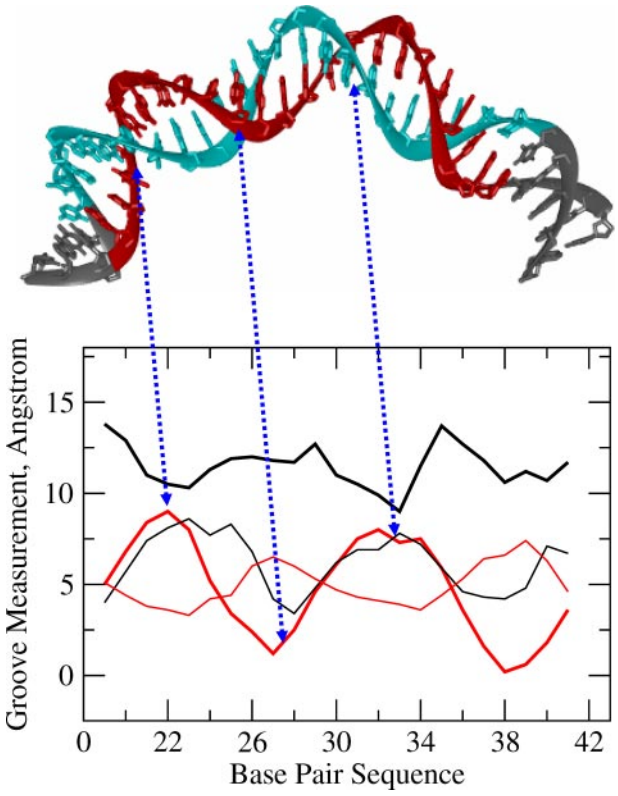

FIGURE 5. **A snapshot of a 30-bp DNA segment extracted from a DNA loop bound with proteins (35) and its helical parameters.** The selected DNA segment involves base pairs 16–45. The major groove width (*thick black*), major groove depth (*thick red*), minor groove width (*thin black*), and minor groove depth (*thin red*) for the middle 23 base pairs (highlighted in *red* and *cyan*) were analyzed. The correspondence between the structure and the helical parameters is shown with the *arrows*. The helical parameters from this segment are quite similar to the ones from the DNA segment that was bent by force.

After 4.5 ns of dynamics simulation for the complex with the Cho DNA sequence, the front dimer shifted further in the same direction (Fig. 4*B*). The dimer-dimer interface apparently preferred a slightly staggered conformation that allowed the dimers to associate favorably without steric conflict between the contacting monomers across the interface. Consistently, the conformational change in this regard was the same for the complex with the Ho DNA sequence (Fig. 4*C*). When viewed through the dimer-dimer interface, it can be seen that in the starting structure, the dimer-dimer interface on both sides was relatively loose (Fig. 6*A*). Comparing with the starting conformation, the left side of the interface became tighter while the right side of the interface changed little for the complex involving the Cho DNA sequence (Fig. 6*B*); however, both sides of the interface became nicely packed when the Ho DNA sequence was used (Fig. 6*C*). It is also visible that the DNA at the center was more compressed for the Ho sequence than for the Cho sequence (data not shown). These results show that the DNA flexibility was important for the p53 dimers to optimize the interactions while maintaining the specific binding to the DNA.

Fig. 7 further shows the atomic details for half of the p53 dimer-dimer interface, representing both cases. The concavity at the joint of turn S7S8 and loop L1 from the top monomer complemented well the molecular contour of the bottom monomers at loop L2, turn S5S6, and the N terminus, with the atomic details showing the favorable interactions. The interaction energies between the p53 dimers for both complexes were also calculated (Fig. 8*A*). In both cases, the interaction energy seems to reach equilibrium after ~4 ns of simulation. On the other hand, the interaction energies between p53 and the central 4 base pairs were very different (Fig. 8*B*). When the system was equilibrated after 6 ns into the trajectory, the interaction energy was much more favorable for the complex involving the Ho DNA sequence than for the complex involving the Cho sequence, indicating the tight packing between the DNA and protein in the former case.

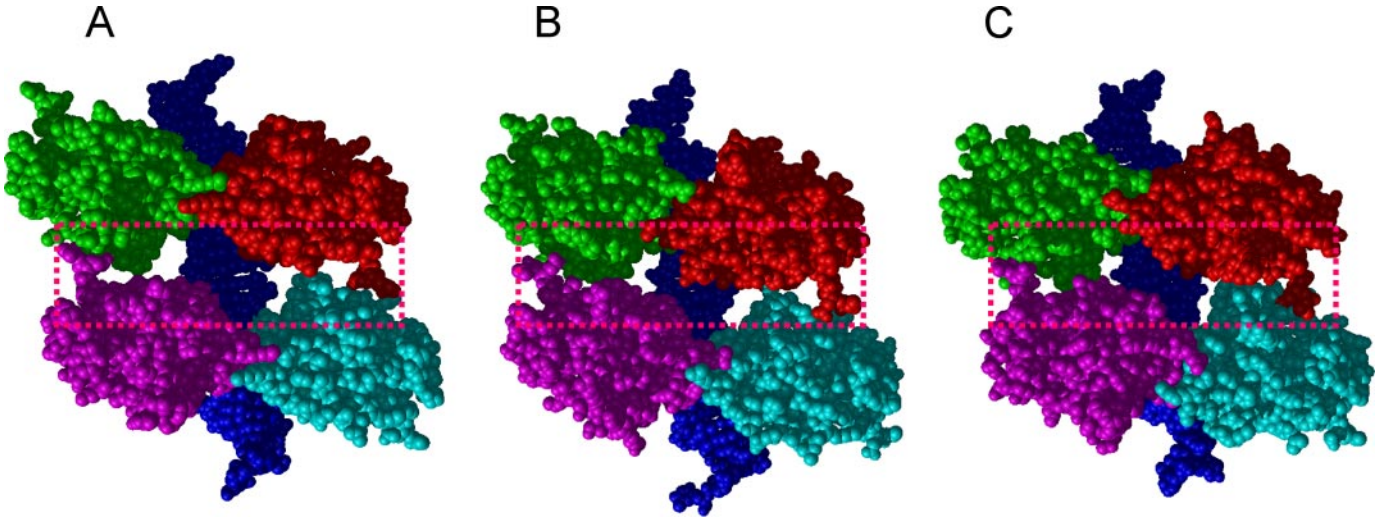

FIGURE 6. **p53 dimer-dimer interactions in the DNA bent conformation.** *A*, starting structure. *B* and *C*, snapshots of the DNA-p53t complexes at 4.5 ns from the simulation involving the Cho DNA sequence and at 7.5 ns from the simulation involving the Ho DNA sequence, respectively. The dimer-dimer interface is *highlighted with boxes*. In the starting structure (*A*), both sides of the interface have limited interaction with large spaces between the dimers. In the complex for the Cho sequence (*B*), the interactions on the left side of the interface are more extensive than the right side whereas in the complex for the Ho sequence (*C*) both sides have more favorable interactions than the starting structure. It is also visible that the DNA is more compact at the center of the DNA for the Ho sequence than for the Cho sequence.

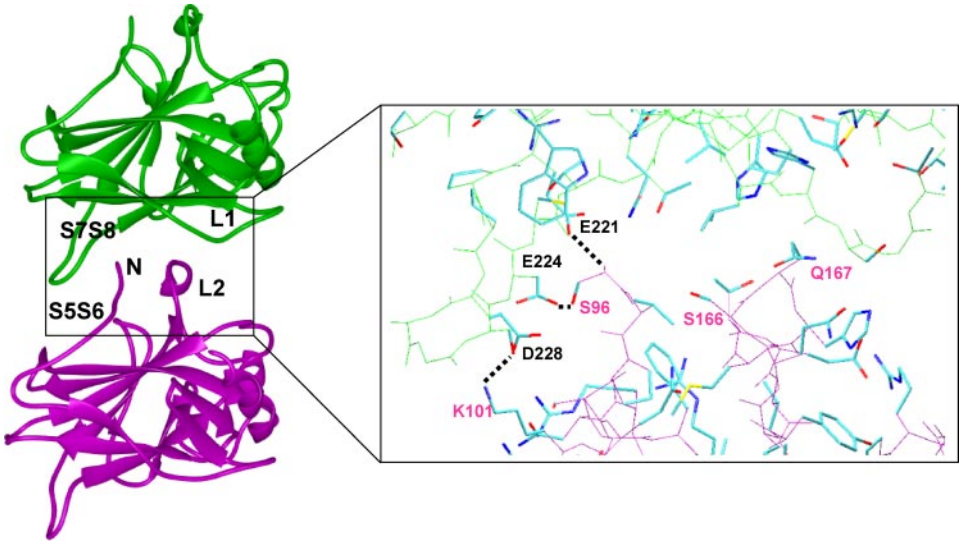

FIGURE 7. **Snapshot of the p53 dimer-dimer interface taken from the complex with the Cho sequence at 5 ns.** The surfaces from each monomer at the interface complement each other well geometrically. The details of the residue interactions are shown to display the hydrogen bonding between several residues on the left and extensive other interaction on the right side of the interface. The backbones of the proteins are *colored* as in Fig. 4 while the atoms N, O, and C in the side chains are colored *blue*, *red*, and *cyan*, respectively.

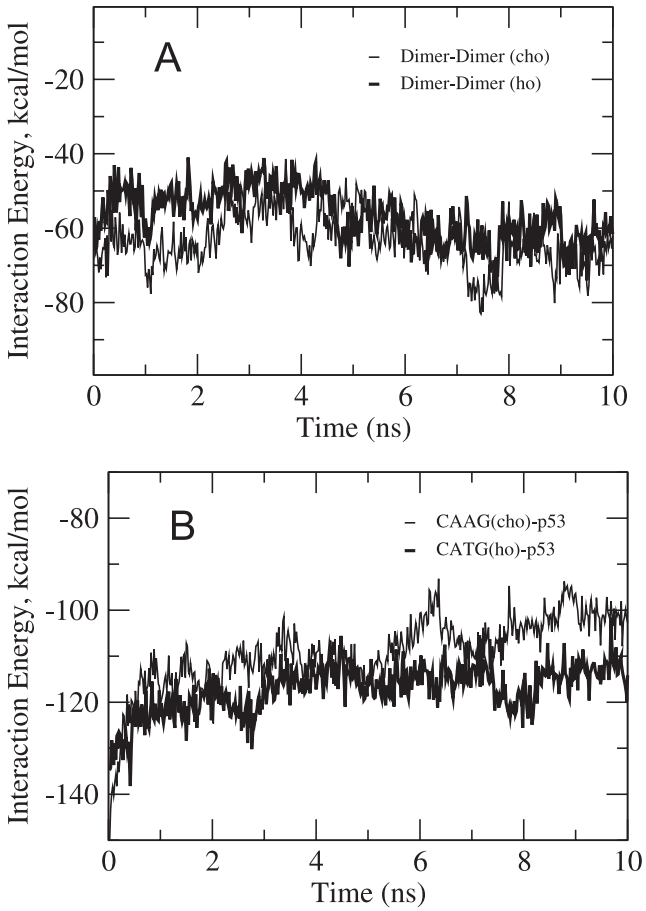

FIGURE 8. **Interaction energy (*kcal/mol*) changes over the 10-ns trajectories between p53 dimers (*A*) and between p53 and the four base pairs at the center of the half site (*B*).** The interactions between the p53 dimers became more favorable overall while the interactions between p53 and DNA became less favorable compared with that in the starting conformation. The more favorable p53-DNA interaction for the Ho sequence indicates the tighter packing than in the complex with the Cho sequence. The interaction energy was calculated with the Charmm program using distance-dependent dielectric constant with a coefficient of 4 and a cutoff of 12 Å for non-bonded interactions.

Tetramer Modeling—We have shown that the forced DNA bending conformations were consistent with the structural parameters of bent DNA conformations from the data base. On the other hand, our simulations were able to observe only moderate DNA bending and a p53 dimer-dimer interface shift from the starting conformation. Experimentally it was shown that the bending can be much larger, particularly in the context of the full-length p53 protein. To bridge this missing link, we attempted to manually dock the p53 tetramer onto the specific DNA consensus site using the DNA conformation that was force bent by ~45°. Fig. 9 shows the docked organization of the complex. Here, we assumed that the specific interaction between p53 and the DNA at the major groove is retained in the DNA bent conformations. Thus, the docked conformation was unique, given the constraints that were imposed for the specific interactions at the major groove. When the dimer-dimer interface in the docked conformation is placed parallel to the surface of the paper, the staggered organization of the p53 dimers is clearly visible (Fig. 9*B*) and is consistent with the simulated DNA-p53t complex conformation (Fig. 4, *B* and *C*). Thus, our combined simulation and docking results suggest that the observed p53 tetramer-DNA complex model is biologically relevant.

The stability of the complex depends on many factors including the DNA sequence (36), the length of the DNA segment, whether full-length p53 protein or its core domains were involved, and possibly the conformational changes within the p53 monomer. The fact that full-length p53 can trigger a larger extent of DNA bending clearly demonstrates the involvement of other protein parts in maintaining the stability of the bent DNA. Thus, the docked conformation may be more relevant to the full-length p53-induced complex structure while the simulation-derived structure corresponds better to the core domain-triggered DNA bending.

DISCUSSION AND CONCLUSIONS

P53 Tetramer-DNA Organization—The p53 tetramer-DNA complex structure and its associated properties have been the focus of several groups in recent years. Unfortunately, no model for the organization of the complex is presented so far with reasonable validation. Recently, a crystal structure of four p53 core domains assembled on two half-site DNA was solved (29), shedding light on the organization of the complex. However, the biological relevance of this structure needs further validation because of the discontinuity of the DNA. If the p53 dimers do bind to the DNA in a specific manner, which was supported by abundant experimental evidence, then the p53 dimers in the DNA-bound state can arguably have only two ways of organization with respect to each other: one of the p53 dimer shifts

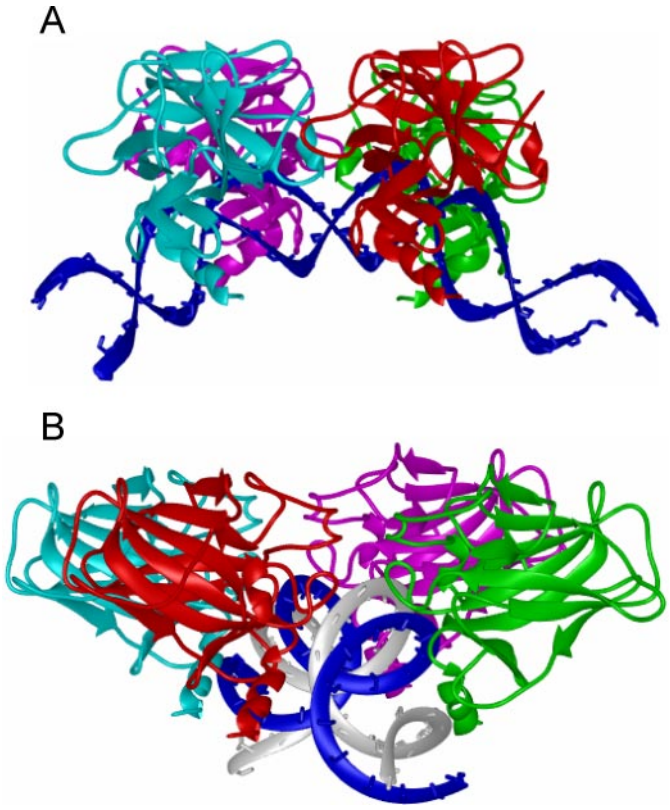

FIGURE 9. **The DNA-p53 tetramer model constructed using the force-bent DNA with a bending angle of ~45° and by fitting the DNA-p53 interface so that the DNA-p53 interaction is in a specific manner.** The constructed model suggests that for the p53 to bind the bent DNA in a specific manner, the p53 dimer in the front has to shift to some extent to satisfy the specific binding requirement, which strongly supports the conclusion derived from the DNA-p53t complex simulation. *Panels A* and *B* are two views perpendicular to each other of the complex.

toward the right, as observed in our simulations (Fig. 4, *B* and *C*), or it moves to the left, as implied in the crystal structure (29). Our simulation results, particularly the initial structure in which the two dimers take a slightly staggered conformation due to the 10.5-bp/turn DNA property, the correlation between the DNA bending extent and the DNA sequence, and the observed tight packing and interaction along the p53 dimer interface, strongly suggest that our proposed model is relevant to biological functions.

DNA Bending—DNA bending upon p53 binding is an important biophysical event. The structural details of DNA bending are crucial to the understanding of the mechanism of selective gene activation and transcriptional activity. Although several groups have determined the extent of DNA bending when bound with p53, the atomic details for how and why the DNA bends are unknown. Based on our results, it is suggested that the p53 dimer-dimer interactions are the major driving force for the DNA bending. However, the extent of interactions and packing at the p53 dimer-dimer interaction depend on the flexibility of the DNA involved. It has been shown that response elements containing CATG base sequence can bend by ~50° upon binding of p53 core domain but response elements containing CTTG base sequence bend only from 25 to 37° (14). The two base sequences used in this work contain a CAAG and a CATG, which bend 20 and 35°, respectively, consistent with the DNA flexibility property. The binding of the p53 dimer alone is therefore mainly responsible for the tight interactions between protein and DNA. It is the dimer-dimer interactions that force the intrinsically flexible DNA to adopt the bent conformations. Our results also suggest that upon further optimization of the dimer-dimer interface interactions and protein-DNA packing, more dramatic DNA bending is possible as long as the DNA flexibility permits.

p53-DNA Binding Cooperativeness—The binding of p53 to DNA is cooperative in that p53 interacts with full site DNA much more strongly than with incomplete p53 binding site. Previous comparative study of the DNA binding with a family of p53 proteins, including p53, p63, and p73, suggests that the cooperative binding is due to the p53 dimerization at the H1 helix interface (37), highlighting the key role of the dimerization of p53 and its binding to DNA. The DNA binding study of p53 modified at the H1 helix also seems to support the importance of the dimerization of p53 to cooperativity (25). However, as we have pointed out, the p53 dimer-dimer interactions and the tighter p53-DNA interactions upon DNA bending may have played more important roles in the cooperativity of p53-DNA binding. In a binding study of p53 to various promoters and DNA recognition, it was found that most of the response elements containing CATG sequence at the center of both half sites correspond to high affinity whereas those containing at least one CAAG or CTTG motif at the center of the half sites correspond mostly to low binding affinities (38). Our results are consistent with their observations. This consistency in turn demonstrates that the favorable interactions at the dimer-dimer interface and the enhanced p53-DNA packing, coupled with the intrinsic DNA flexibility, are responsible for the cooperative nature of p53-DNA binding.

In summary, our simulation results provided a p53-DNA complex model with many features that are consistent with experimental observations and therefore are likely to be biologically relevant. Our results also reveal important atomic details and the underlying mechanism for DNA bending and the cooperative nature for p53-DNA interactions.

Acknowledgments—We thank Z. Shakked for communicating results prior to publication. This study utilized the high performance computational capabilities of the Biowulf PC/Linux cluster at the National Institutes of Health, Bethesda, MD (biowulf.nih.gov).

Note Added in Proof—We were just made aware that in a chapter not indexed by Medline further details of the Nagaich *et al.* (15) model of the p53 complex with DNA illustrating bending at the half-site centers, between the half-sites (overall bend of 40°), and 2 Å sliding between the two half-sites were provided by Durell *et al.* (39).

REFERENCES

1. Kastan, M. B., Onyekwere, O., Sidransky, D., Vogelstein, B., and Craig, R. W. (1991) *Cancer Res.* **51,** 6304–6311
2. Vousden, K. H. (2002) *Biochim. Biophys. Acta* **1602,** 47–59
3. Vousden, K. H., and Lu, X. (2002) *Nat. Rev. Cancer* **2,** 594–604
4. el-Deiry, W. S. (1998) *Semin. Cancer Biol.* **8,** 345–357
5. Bargonetti, J., Friedman, P. N., Kern, S. E., Vogelstein, B., and Prives, C. (1991) *Cell* **65,** 1083–1091
6. Balagurumoorthy, P., Sakamoto, H., Lewis, M. S., Zambrano, N., Clore,

G. M., Gronenborn, A. M., Appella, E., and Harrington, R. E. (1995) *Proc. Natl. Acad. Sci. U. S. A.* **92,** 8591–8595
7. el-Deiry, W. S., Kern, S. E., Pietenpol, J. A., Kinzler, K. W., and Vogelstein, B. (1992) *Nat. Genet.* **1,** 45–49
8. Balagurumoorthy, P., Lindsay, S. M., and Harrington, R. E. (2002) *Biophys. Chem.* **101–102**, 611–623
9. Funk, W. D., Pak, D. T., Karas, R. H., Wright, W. E., and Shay, J. W. (1992) *Mol. Cell Biol.* **12,** 2866–2871
10. Fields, S., and Jang, S. K. (1990) *Science* **249,** 1046–1049
11. Cho, Y., Gorina, S., Jeffrey, P. D., and Pavletich, N. P. (1994) *Science* **265,** 346–355
12. Clore, G. M., Omichinski, J. G., Sakaguchi, K., Zambrano, N., Sakamoto, H., Appella, E., and Gronenborn, A. M. (1994) *Science* **265,** 386–391
13. McKinney, K., Mattia, M., Gottifredi, V., and Prives, C. (2004) *Mol. Cell* **16,** 413–424
14. Nagaich, A. K., Appella, E., and Harrington, R. E. (1997) *J. Biol. Chem.* **272,** 14842–14849
15. Nagaich, A. K., Zhurkin, V. B., Durell, S. R., Jernigan, R. L., Appella, E., and Harrington, R. E. (1999) *Proc. Natl. Acad. Sci. U. S. A.* **96,** 1875–1880
16. Cherny, D. I., Striker, G., Subramaniam, V., Jett, S. D., Palecek, E., and Jovin, T. M. (1999) *J. Mol. Biol.* **294,** 1015–1026
17. Ceskova, P., Chichger, H., Wallace, M., Vojtesek, B., and Hupp, T. R. (2006) *J. Mol. Biol.* **357,** 442–456
18. Weinberg, R. L., Veprintsev, D. B., and Fersht, A. R. (2004) *J. Mol. Biol.* **341,** 1145–1159
19. Stenger, J. E., Tegtmeyer, P., Mayr, G. A., Reed, M., Wang, Y., Wang, P., Hough, P. V., and Mastrangelo, I. A. (1994) *EMBO J.* **13,** 6011–6020
20. Wang, Y., Schwedes, J. F., Parks, D., Mann, K., and Tegtmeyer, P. (1995) *Mol. Cell. Biol.* **15,** 2157–2165
21. Waterman, J. L., Shenk, J. L., and Halazonetis, T. D. (1995) *EMBO J.* **14,** 512–519
22. McLure, K. G., and Lee, P. W. (1998) *EMBO J.* **17,** 3342–3350
23. Nagaich, A. K., Zhurkin, V. B., Sakamoto, H., Gorin, A. A., Clore, G. M., Gronenborn, A. M., Appella, E., and Harrington, R. E. (1997) *J. Biol. Chem.* **272,** 14830–14841
24. Klein, C., Planker, E., Diercks, T., Kessler, H., Kunkele, K. P., Lang, K., Hansen, S., and Schwaiger, M. (2001) *J. Biol. Chem.* **276,** 49020–49027
25. Sun, X. Z., Vinci, C., Makmura, L., Han, S., Tran, D., Nguyen, J., Hamann, M., Grazziani, S., Sheppard, S., Gutova, M., Zhou, F., Thomas, J., and Momand, J. (2003) *Antioxid. Redox. Signal.* **5,** 655–665
26. Rippin, T. M., Freund, S. M., Veprintsev, D. B., and Fersht, A. R. (2002) *J. Mol. Biol.* **319,** 351–358
27. Dehner, A., Klein, C., Hansen, S., Muller, L., Buchner, J., Schwaiger, M., and Kessler, H. (2005) *Angew Chem. Int. Ed. Engl.* **44,** 5247–5251
28. Ma, B., Pan, Y., Gunasekaran, K., Venkataraghavan, R. B., Levine, A. J., and Nussinov, R. (2005) *Proc. Natl. Acad. Sci. U. S. A.* **102,** 3988–3993
29. Kitayner, M., Rozenberg, H., Kessler, N., Rabinovich, D., Shaulov, L., Haran, T. E., and Shakked, Z. (2006) *Mol. Cell* **22,** 741–753
30. Lebrun, A., Lavery, R., and Weinstein, H. (2001) *Protein Eng.* **14,** 233–243
31. Ho, W. C., Fitzgerald, M. X., and Marmorstein, R. (2006) *J. Biol. Chem.* **281,** 20494–20502
32. Jorgensen, W. L., Chandrasekhar, J., Madura, J. D., Impey, R. W., and Klein, M. L. (1983) *J. Chem. Phys.* **79,** 926–935
33. Brooks, B. R., Bruccoleri, R. E., Olafson, B. D., States, D. J., Swaminathan, S., and Karplus, M. (1983) *J. Comput. Chem.* **4,** 187–217
34. MacKerell, A. D., Jr., Bashford, D., Jr., Bellott, M., Dunbrack, R. L., Jr., Evanseck, J. D., Field, M. J., Fischer, S., Gao, J., Guo, H., Ha, S., Joseph-McCarthy, D., Kuchnir, L., Kuczera, K., Lau, F. T. K., Mattos, C., Michnick, S., Ngo, T., Nguyen, D. T., Prodhom, B., Reiher, W. E., III, Roux, B., Schlenkrich, M., Smith, J. C., Stote, R., Straub, J., Watanabe, M., Wiorkiewicz-Kuczera, J., Yin, D., and Karplus, M. (1998) *J. Phys. Chem. B* **102,** 3586–3616
35. Luger, K., Mader, A. W., Richmond, R. K., Sargent, D. F., and Richmond, T. J. (1997) *Nature* **389,** 251–260
36. Nadeau, J. G., and Crothers, D. M. (1989) *Proc. Natl. Acad. Sci. U. S. A.* **86,** 2622–2626
37. Klein, C., Georges, G., Kunkele, K. P., Huber, R., Engh, R. A., and Hansen, S. (2001) *J. Biol. Chem.* **276,** 37390–37401
38. Weinberg, R. L., Veprintsev, D. B., Bycroft, M., and Fersht, A. R. (2005) *J. Mol. Biol.* **348,** 589–596
39. Durell, S. R., Jernigan, R. L., Apella, E., Nagaich, A. K., Harrington, R. E., and Zhurkin, V. B. (1998) *Proceedings of the Tenth Conversation, Albany, June 17–21, 1997* (Sarma, R. H., and Sarma, M. H., eds) pp. 277–295, SUNY, Albany, NY

Structural Basis for p53 Binding-induced DNA Bending

Yongping Pan and Ruth Nussinov

J. Biol. Chem. 2007, 282:691-699.
doi: 10.1074/jbc.M605908200 originally published online November 3, 2006

Supplemental information

Figure S1. The helical parameters for the 15-bp DNA segment in free form (black), in bound with p53 monomer (red) and in bound with p53 dimer (green). For each comparison, major groove width, depth, minor groove width and depth were plotted separately in (A), (B), (C) and (D). Only the half site consensus base pairs were shown for clarity.

Figure S2. DNA helical parameters for the full 20-bp binding site when the DNA segment was simulated alone without constraint (black), when forced to bend (green), when bound with p53 tetramer with the Cho DNA sequence (red), and when bound with p53 tetramer with Ho DNA sequence (blue). Forced DNA bending was achieved by applying a distance constraint between the centers of masses of the three nucleotides at each end of the DNA molecule with a force constant of 500 kcal/mol/Å with a distance decrement of 0.25 Å and equilibrated for 25 ps at each step. The parameters for the bent DNA by force were averaged over a range of bent angles from 0 to 90 degrees while the other two sets of parameters were averaged over the last 5 ns from the 10 ns MD trajectories.

Figure S1

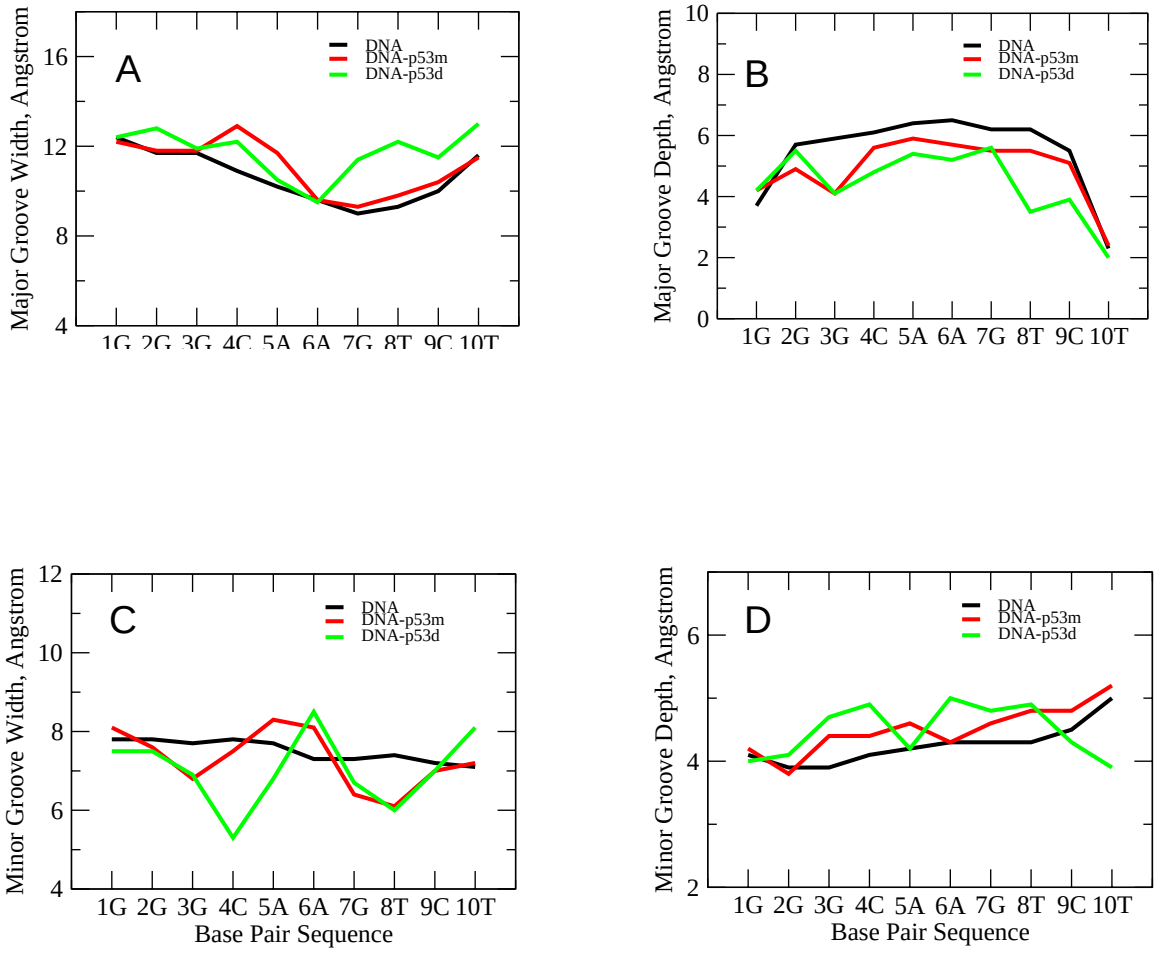
A
B
C
D
DNA
DNA-p53m
DNA-p53d
Major Groove Width, Angstrom
Major Groove Depth, Angstrom
Minor Groove Width, Angstrom
Minor Groove Depth, Angstrom
1G 2G 3G 4C 5A 6A 7G 8T 9C 10T
Base Pair Sequence

Figure S2

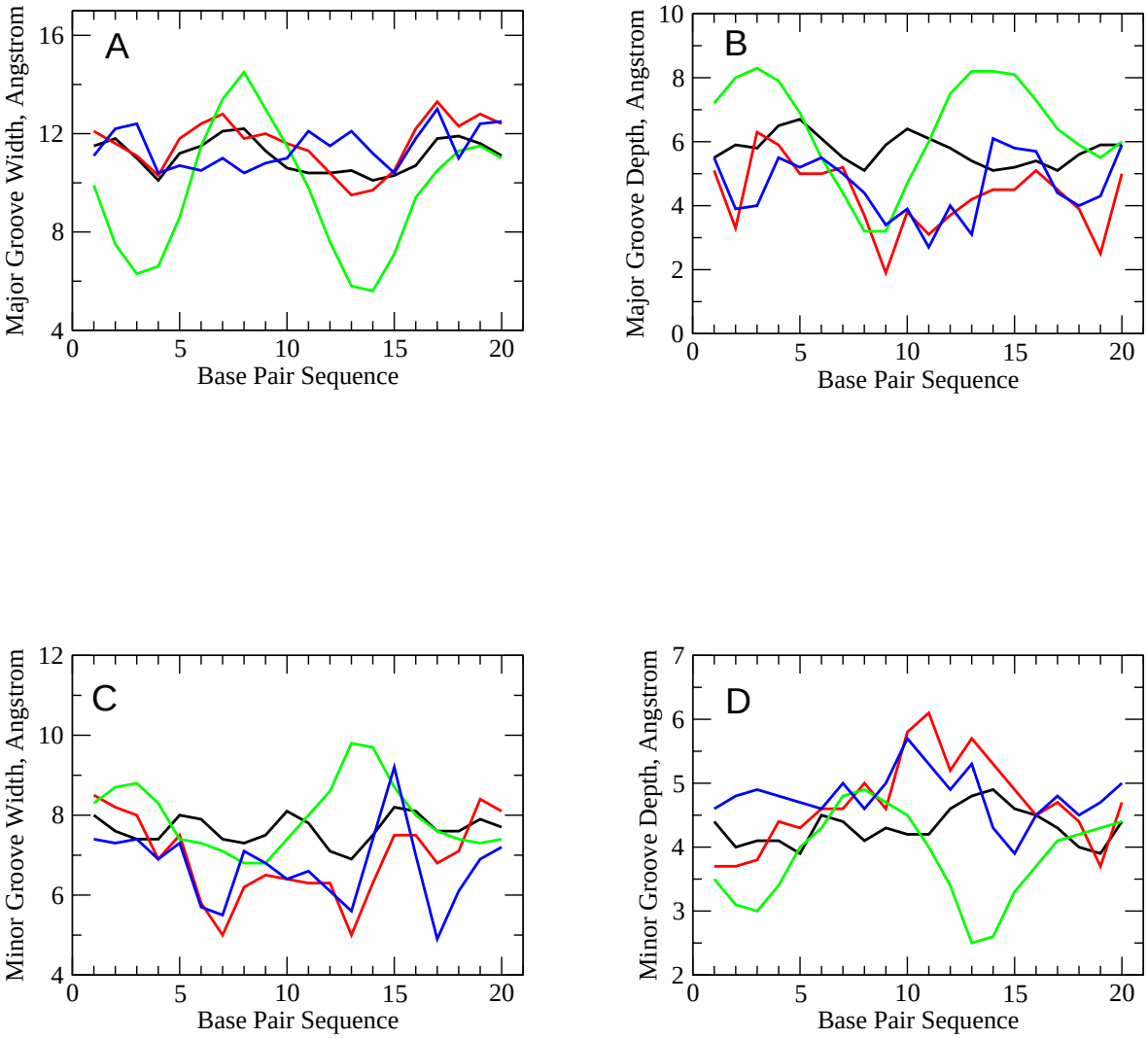
A
Major Groove Width, Angstrom
Base Pair Sequence
B
Major Groove Depth, Angstrom
Base Pair Sequence
C
Minor Groove Width, Angstrom
Base Pair Sequence
D
Minor Groove Depth, Angstrom
Base Pair Sequence